Carbohydrate Polymers 105 (2014) 285–292

Contents lists available at ScienceDirect

Carbohydrate Polymers

journal homepage: www.elsevier.com/locate/carbpol

Hybrid HPMC nanocomposites containing bacterial cellulose nanocrystals and silver nanoparticles

Johnsy George[a,*], Ranganathan Kumar[a], Vallayil Appukuttan Sajeevkumar[a], Karna Venkata Ramana[a], Ramalingam Rajamanickam[a], Virat Abhishek[a], Shanmugam Nadanasabapathy[a], Siddaramaiah[b]

[a] Defence Food Research laboratory, Siddarthanagar, Mysore, 570 011, India
[b] Sri Jayachamarajendra College of Engineering, Mysore, 570 006, India

ARTICLE INFO

Article history:
Received 12 November 2013
Received in revised form 8 January 2014
Accepted 16 January 2014
Available online 31 January 2014

Keywords:
Hybrid nanocomposites
Cellulose nanocrystals
Silver nanoparticles

ABSTRACT

Hydroxypropyl methyl cellulose (HPMC) based hybrid nanocomposites reinforced with bacterial cellulose nanocrystals (BCNC) and silver nanoparticles (AgNPs) had been prepared and characterised. BCNC was capable of improving the tensile strength and modulus of HPMC, but they made the film more brittle. The addition of AgNPs along with BCNC, helped to regain some of the lost elongation properties without affecting other properties. Moisture sorption analysis proved that the hydrophilicity of the nanocomposite decreased considerably by the addition of these nanomaterials. Several mathematical models were also used to fit the experimental sorption results. A unique combination of two nanomaterials was highly effective in overcoming certain limitations of nanocomposites which uses only one type of nanomaterial. This type of hybrid nanocomposites with superior properties is expected to be useful in eco-friendly food packaging applications.

1. Introduction

The efficacy of cellulose and its derivatives in bio-based packaging applications were evaluated extensively as an alternative to non degradable synthetic plastics. These bio-based polymers are attractive alternatives to the existing packaging materials due to their biodegradability, renewability and large scale availability at relatively low cost. Among the cellulose derivatives, HPMC is a good film forming material and has lots of potential in food packaging applications, due to its flexibility, transparency and resistance to oils and fats (Krochta & Mulder-Johnston, 1997). Moreover, HPMC is approved for food applications, which makes it suitable for preparing edible film and coatings (Brindle & Krochta, 2008). However, the hydrophilic nature of this polymer results in loss of barrier properties when exposed to moisture or even a solubilisation into food with high-water activities (Bertuzzi, Armada, & Gottifredi, 2007). Several hydrophobic additives such as long chain fatty acids had been incorporated into HPMC, to reduce its moisture affinity and water vapour transmission (Ayranci & Tunc, 2001; Villalobos, Hernandez-Munoz, & Chiralt, 2006). However, the presence of hydrophobic additives within a hydrophilic polymer matrix can lead to phase separation and tends to give films having a "two-layer-like" structure (Phan et al., 2002). Similarly the presence of lipid layers can reduce the mechanical properties of the film and increases the possibility of migration of these additives into the food systems (Fahs, Brogly, Bistac, & Schmitt, 2010). Crosslinking HPMC, using agents like polycarboxylic acid is another widely employed technique to reduce the moisture sensitivity; however, the mechanical properties of the polymer will be significantly reduced. It was reported that the percentage elongation of citric acid crosslinked HPMC films were reduced by about 58–70% with the introduction of crosslinks (Sebti, Delves-Broughton, & Coma, 2003). This reduction in the percentage elongation at break mainly attributed to the cross links, made the biopolymer film more rigid and brittle. Hence, alternate routes have to be explored to reduce the moisture affinity of HPMC without compromising its mechanical properties.

The applications of polymer nanocomposites were rapidly expanding with the advent of several novel nanomaterials that can impart superior properties to polymers by reinforcing them. Combination of nanotechnology and polymer technology is imperative in amalgamating multifunctional attributes together in a single polymer matrix to address the short comings of already existing materials. The main advantage of nanoparticles in polymer reinforcement is that they are capable of inducing unique and better properties even at relatively low concentration in comparison with other conventional reinforcing agents. Nanocomposites of biopolymers are very promising especially in the field of food packaging as

* Corresponding author. Tel.: +91 821 2473150; fax: +91 821 2473468.
E-mail address: g.johnsy@gmail.com (J. George).

0144-8617/$ – see front matter © 2014 Elsevier Ltd. All rights reserved.
http://dx.doi.org/10.1016/j.carbpol.2014.01.057

they offer better properties coupled with eco-friendly attributes (Sorrentino, Gorrasi, & Vittoria, 2007). Reinforcing biopolymers with nanoparticles is an excellent way to overcome some of the shortcomings of such polymers, which limits their use in food packaging applications. Among the nanoparticles, cellulose nanocrystals attracted a great deal of interest in such applications, due to its nano scale dimensions, highly crystalline nature, a high aspect ratio, low cost, renewability and biodegradability (George & Siddaramaiah, 2012; Pandey, Nakagaito, & Takagi, 2013). Cellulose nanocrystals are generally obtained by the acid hydrolysis of cellulose micro fibrils. Cellulose micro fibrils are composed of highly ordered crystalline and less ordered "amorphous" domains, which can be preferentially separated by employing controlled hydrolysis. Less ordered amorphous regions are more susceptible to acid hydrolysis in contrast to crystalline fractions and during hydrolysis these micro fibrils break down into highly ordered, rod shaped crystalline fractions. Because of their nano dimensions and shape, these crystalline fractions obtained from hydrolysis route are known as cellulose nanocrystals (Habibi, Lucia, & Rojas, 2010).

Cellulose obtained from microbial sources are more preferred over plant cellulose in novel and specific applications as it is available in relatively pure form, exhibits a higher degree of polymerization, high crystallinity and better properties (Iguchi, Yamanaka, & Budhino, 2000). In this context, bacterial cellulose that can be converted in to nanocrystals with a good aspect ratio is gaining great importance in the field of bionanocomposites. Cellulose nanocrystals can form load-bearing, percolated network like architecture within the polymer matrix, because of the presence of strongly interacting surface hydroxyl groups which increases filler-filler interactions (Shanmuganathan, Capadona, Rowan, & Weder., 2010). The significant reinforcement observed for cellulose nanocrystal incorporated nanocomposites can also be attributed to the interactions between the polymer matrix and the nanocrystals. These types of matrix-filler interactions are more prominent in water soluble and other hydrophilic polymers, where the nanocrystals can attain a high level of dispersion in polymer matrix. However, cellulose nanocrystals incorporated polymer nanocomposites also have some drawbacks, at least partly, due to the reduced elongation at break and moisture sensitivity. By using another reinforcing nanomaterial such as silver nanoparticles (AgNPs) in combination with cellulose nanocrystals can be beneficial in overcoming some of these draw backs.

The feasibility of using metallic nanomaterials like AgNPs in the development of antimicrobial food packaging materials was extensively studied. Many organic polymers were found to be good host materials for the synthesis and stabilisation of AgNPs. This type of polymer assisted synthesis route also provides a simple, eco friendly and cost effective technique for the stabilisation of AgNPs. HPMC is one such polymer that can stabilise silver nanoparticles in large quantities (Tai, Wang, Tai, & Liu, 2009). AgNPs are known to improve several properties of HPMC apart from imparting antimicrobial properties (Moura et al., 2012). In this study, we report a simple method to overcome the limitations of cellulose nanocrystals reinforced HPMC bionanocomposites by using AgNPs along with cellulose nanocrystals. The spectral characteristics, morphology, mechanical properties and moisture sorption behaviour of these nanocomposite films were investigated. The results suggested that a combination of two nanoparticles together in a single polymer matrix can impart better mechanical strength and moisture resistance, which makes these hybrid nanocomposites superior to other bio-based materials. In addition, this method represents a promising route for creating innovative materials, in particular by enhancing the ductile properties of nanocomposites in applications where flexibility is very essential.

2. Experimental

2.1. Materials

Bacterial cellulose as pellicles was prepared from '*Gluconacetobacter xylinus*' as reported earlier (George, Ramana, Sabapathy, Jagannath, & Bawa, 2005). These pellicles were purified by boiling in 0.2 M aqueous NaOH solution for 30 min followed by rinsing with distilled water. The purified pellicles were mechanically disintegrated to cellulose micro fibrils using a laboratory blender (5000–6000 rpm). These micro fibrils were converted into nanocrystals by hydrolyzing with hydrochloric acid (HCl). 500 mL of 4 N HCl (Reagent grade 36%, Fisher Scientific, India) was added to 100 g of cellulose micro fibrils and allowed hydrolyzing for about 4 h in boiling conditions. The BCNC suspension formed was then centrifuged at 5000 rpm for 5 min and washed with distilled water to remove the acid. Cellulose nanocrystals at different concentrations (2 and 4 wt%) were prepared separately in 100 mL distilled water by ultrasonication at 80% amplitude, which provided necessary mechanical agitation to disperse the agglomerated nanocrystals. HPMC powder with hydroxy propyl content of 8.2% was procured from M/s Loba Chemie, India and its solution were prepared by dissolving 10 g in 100 mL distilled water at 65 °C. HPMC–BCNC nanocomposites were prepared by the addition of BCNC to a calculated quantity of HPMC solution (100 mL) followed by stirring and ultrasonication for 30 min. The nanocomposite solutions were casted in polypropylene petri dishes and dried at 37 °C for 48 h and used for further characterization. AgNPs were synthesized within the polymer in the presence of BCNC by reducing silver salt ($AgNO_3$, Sigma Chemical Co., USA) using a reducing agent like $NaBH_4$ (Sigma Chemical Co., USA). During the preparation, 3 mL of aqueous $AgNO_3$ (10 mmol) was added to the HPMC solution and stirred well followed by the drop wise addition of 3 mL $NaBH_4$ (10 mmol). The quantity of AgNPs was fixed at 1 wt% for all combinations. The formation of silver nanoparticles by the reduction of $AgNO_3$ was confirmed by the characteristic bright yellow colour of the polymer solution.

2.2. Methods

UV–vis absorption spectra of HPMC nanocomposites containing BCNC and AgNPs were recorded using a Spectronic UV–vis spectrometer (Model: Genesys 2, USA). The morphology of the HPMC nanocomposites was studied using Transmission electron microscope (JEM 3010, JEOL, Japan) and atomic force microscope (Solver PRO-M NT-MDT, Ireland). A very dilute nanocomposite suspension containing AgNPs was dropped casted on a carbon coated Cu grid, and TEM images were obtained at an accelerating voltage of 300 kV. In the case of the AFM, a drop of very dilute nanocomposite suspension (0.05 wt/wt) was allowed to dry at room temperature overnight on a freshly cleaved mica substrate. The images were acquired with silicon cantilevers (NSG-01) in non-contact mode. The resonant frequency of the cantilever was 87–230 kHz. The IR spectra of the nanocomposite samples were recorded using an FTIR spectrometer (Thermo Nicolet FTIR, Model 5700, Madison, WI) fitted with a single bounce attenuated total reflectance (ATR) accessory with ZnSe crystal. X-ray diffraction studies were conducted using an X-ray diffractometer (D2 Phaser, Bruker AXS, Germany) operating at 30 kV and 10 mA. The diffraction patterns were recorded using Cu-Kα radiation and the film samples were analyzed at a 2θ range, 1–50°. The percentage crystallinity was estimated based on the area under the curve of crystalline and amorphous regions using TOPAS^{TM} software, supplied along with the X-ray diffractometer. The average crystal size (L) was determined by Scherrer's equation, where FWHM is the full width at half

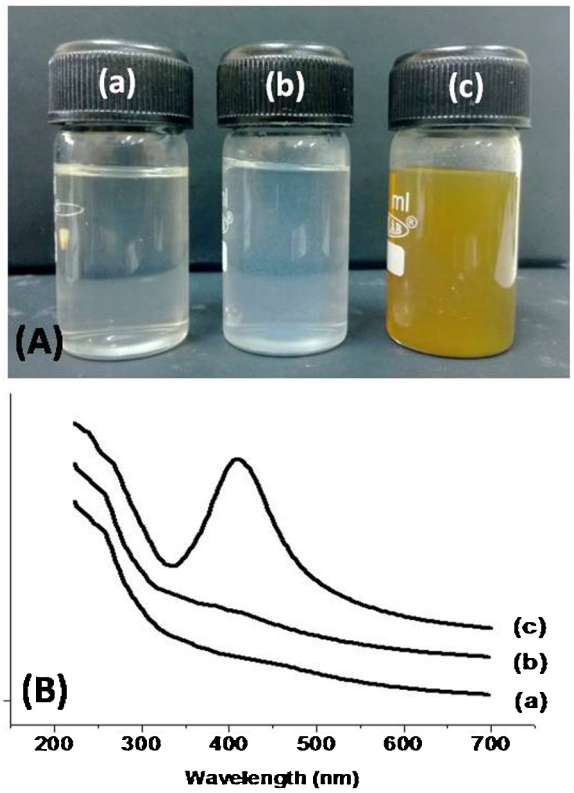

Fig. 1. (A) Optical image and (B) corresponding UV–vis absorption spectra of (a) HPMC, (b) HPMC–BCNC nanocomposite and (c) HPMC–BCNC nanocomposite containing AgNPs.

maximum of diffraction peaks, K is the Scherrer constant (0.89), λ is the wavelength of X-ray source and θ is Bragg's angle.

$$\mathrm{FWHM}(2\theta) = \frac{K\lambda}{L/\cos\theta} \quad (1)$$

Mechanical properties of HPMC nanocomposite films were evaluated in tensile mode using a UTM (Model: LRX Plus, Lloyd Instruments, UK) with a gauge length of 25 mm and cross head speed of 100 mm/min. Samples were cut into rectangular strips with dimensions of $5'' \times 1''$ as per ASTM D 882 standards and five strips were tested for each sample. A moisture sorption analyzer (Q 5000 SA, TA Instruments, USA) was used to study the moisture sorption properties under controlled conditions of temperature and humidity. The stepwise adsorption studies of the film samples were carried out from 10% to 90% RH at a step interval of 10% RH at 25 °C. At each RH level, equilibration was stopped when the relative change in sample mass remained below 0.01% for 5 min, and the next RH step was automatically applied.

3. Results and discussion

3.1. Fabrication of hybrid nanocomposites

Bio-based hybrid nanocomposites were prepared by incorporating a unique combination of two nanomaterials such as BCNC and AgNPs in HPMC matrix. The optical images of HPMC and its nanocomposites in water and their corresponding UV–vis absorption spectra are depicted in Fig. 1. HPMC forms a clear solution with water, while the addition of BCNC had resulted in a cloudy appearance. The addition of $AgNO_3$ and $NaBH_4$ into the system resulted in changing the colour of the suspension to bright yellow, confirming the formation of AgNPs (Fig. 1A). The uniform distribution of yellow colour throughout the suspension also implies that AgNPs were uniformly distributed throughout the nanocomposite matrix. For the AgNPs containing nanocomposite suspension, the characteristic plasmon band was observed at 410 nm, which again confirmed the formation of silver nanoparticles (Fig. 1B).

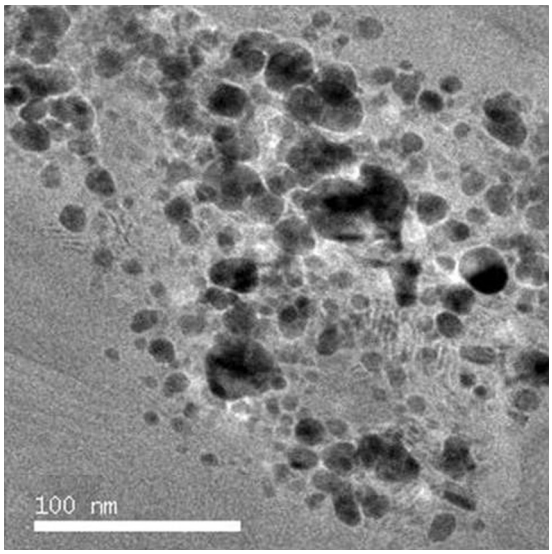

Fig. 2. TEM image of HPMC nanocomposite containing 4 wt% BCNC and 1 wt% AgNPs.

3.2. Morphological analysis

The morphology of hybrid nanocomposites was analyzed using TEM and AFM. A representative TEM micrograph of hybrid nanocomposites (Fig. 2) revealed that AgNPs are dispersed well within the polymer matrix. The hydroxyl groups of HPMC strongly interact with silver cations and subsequently stabilises AgNPs. From the image, it is also visible that AgNPs show good contrast with the polymer, while BCNC shows less contrast. AFM images revealed rod shaped bacterial cellulose nanocrystals, which were uniformly distributed throughout the HPMC matrix (Fig. 3A). Moderate aggregation of nanocrystals within the polymer matrix is also visible, which implies the existence of certain interactions among nanocrystals. The aggregation tendency of nanocrystals is mainly due to the existence of strong hydrogen bonding between the surface hydroxyl groups of cellulose. This type of aggregation may lead to the formation of percolated networks, which enhances the mechanical properties of polymer nanocomposites. The addition of AgNPs altered the morphology of nanocomposites, as some of the AgNPs was attached to the BCNC as visible from the AFM images (Fig. 3B). Both HPMC and BCNC are having abundant hydroxyl groups that can stabilise a large amount of metallic nanoparticles.

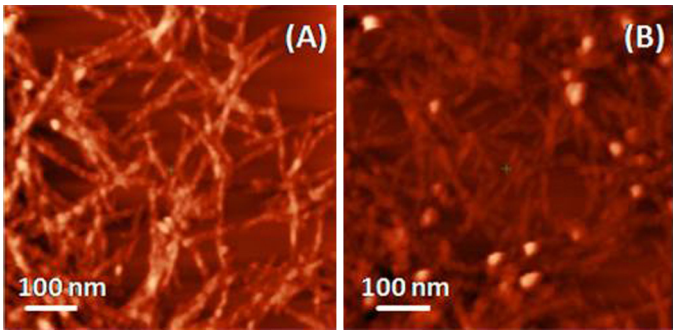

Fig. 3. AFM images of (A) HPMC nanocomposites containing BCNC and (B) HPMC nanocomposite containing both BCNC and AgNPs.

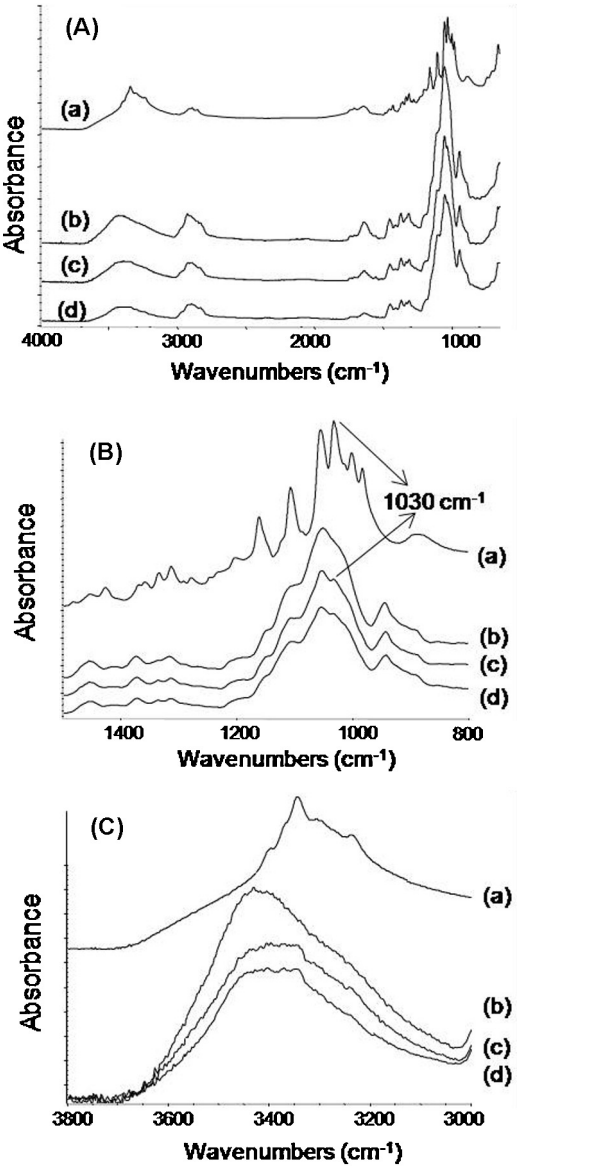

Fig. 4. FTIR spectra of (a) BCNC, (b) HPMC, (c) HPMC + 4 wt% BCNC and (d) HPMC + 4wt % BCNC + 1 wt% AgNPs in the range (A) 4000–650 cm^{-1} (B) 1400–800 cm^{-1} and (C) 3800–3000 cm^{-1}.

The nanoparticles formed in this way will remain attached to the polymer matrix and alters some of the nanocomposite properties.

3.3. FTIR analysis

The FTIR spectra of BCNC, HPMC and its nanocomposites are depicted in Fig. 4. In the spectrum of BCNC, the broad band observed around 3340 cm^{-1} corresponds to the —OH stretching vibrations of cellulose and water molecules, while the band observed at 2893 cm^{-1} is due to the C—H stretching vibrations (Fig. 4A (a)). The band at 1623 cm^{-1} is due to the stretching vibration of C=O groups of cellulose rings as well as the H—OH bending vibrations of adsorbed water molecules. The peak at 1160 cm^{-1} corresponds to the C—C stretching, which is the asymmetric ring breathing mode while 1106 cm^{-1} band corresponds to glycosidic C—O—C stretching vibration. The band at 1055 cm^{-1} and 1030 cm^{-1} correspond to the C—OH stretching vibration of secondary and primary alcohols of cellulose, respectively. HPMC, which is also cellulose based polymer, possess a spectrum much similar to that of BCNC. Here the —OH stretching vibrations were observed as a broad band centered at 3430 cm^{-1} while the band observed around 2900 cm^{-1} corresponds to the stretching vibrations of methyl and hydroxypropyl groups (Fig. 4A (b)). The band at 1645 cm^{-1} is due to the bending vibrations of H—OH groups as well as the stretching vibrations of C=O groups present in HPMC. A broad band visible in the range 1100–1000 cm^{-1} corresponds to the C—C and C—O vibrations of cellulose. The obtained IR bands of both bacterial cellulose and HPMC as shown in Fig. 3A were in a good agreement with previous reports (George et al., 2008; Wang, Dong, & Xu, 2007). The FTIR spectrum of HPMC – 4 wt% BCNC nanocomposite is given in Fig. 4A (c). The addition of BCNC has not affected the IR spectrum of HPMC considerably as visible from the spectrum. This is because both the polymer and reinforcing nanofiller are cellulose based materials. However, the emergence of a band at 1030 cm^{-1} was observed after the addition of BCNC, which is clearly visible in the spectra (Fig. 4B (c)). This is due to the C—OH stretching vibration of primary alcohols present in bacterial cellulose, which also gives some evidence for the formation of nanocomposites. Another difference observed in the spectra was around 3600–3200 cm^{-1}, which corresponds to the stretching vibrations of —OH groups (Fig. 4C (c)). In the case of HPMC, the peak position of —OH stretching band is centered at 3430 cm^{-1}, while that of BCNC is at 3340 cm^{-1}. This difference can be attributed to the strong hydrogen bonding existing in BCNC compared to HPMC. By the addition of BCNC into HPMC, the hydrogen bonding pattern of HPMC also changed as evidenced from the spectra (Fig. 4C (c)). The broad band was shifted to a lower wave length, which suggests that the addition of BCNC enhanced the concentration of strongly hydrogen bonded —OH groups in the HPMC or in other words strong inter molecular interactions through hydrogen bonding were existing between BCNC and HPMC. Similar results were reported earlier, where the absorption band of —OH groups of HPMC at 3448 cm^{-1} was shifted to a lower wave number of 3305 cm^{-1} when nanogels with poly acrylic acid were formed (Yao, Xu, Lu, & Deng, 2011). These types of interactions can also contribute to the improved mechanical properties of nanocomposites (Dogan & McHugh, 2007). The addition of AgNPs on the other hand affected the nanocomposites in a different way. The FTIR analysis revealed a shift in the broad band of —OH groups to a higher wavelength and resulted in a change in this band shape (Fig. 4C (d)). The hydroxyl groups present in HPMC and BCNC play an important role in stabilizing or capping the Ag nanoparticles. During the formation of AgNPs, some of the intermolecular hydrogen bonds of HPMC and BCNC were disrupted, and these hydroxyl groups will be strongly interacting with AgNPs, making it unavailable for other molecules to interact. Similar type of shifting of —OH bands to a higher wavelength in the presence of AgNPs were reported previously (George, Sajeevkumar, Ramana, Sabapathy, & Siddaramiah, 2012).

3.4. X-ray diffraction analysis

The X-ray diffraction patterns of BCNC, HPMC and its nanocomposites are shown in Fig. 4. BCNC exhibited three main peaks at 15.12°, 17.40° and 22.71° (Fig. 5a), which correspond to the diffraction peaks of cellulose-I crystal planes (1 0 1), (1 0 $\bar{1}$) and (0 0 2) respectively (Xu et al., 2013). Other diffraction parameters such as main peak angles (2θ), d-spacing, full width at half maximum, average crystal size and crystallinity index are summarised in Table 1. HPMC exhibited two main diffraction peaks at 7.38° and 19.65°, which corresponds to the diffraction peaks of cellulose crystal planes (1 0 1) and (0 0 2) respectively (Fig. 5b). The diffraction peaks of HPMC are very broad, which indicated their semi-crystalline nature. Furthermore, HPMC possesses much smaller crystallite size and larger d-spacing compared to that of BCNC, which is also indicated its amorphous nature. The addition of 2 and 4 wt% of BCNC made significant differences in the diffraction patterns of

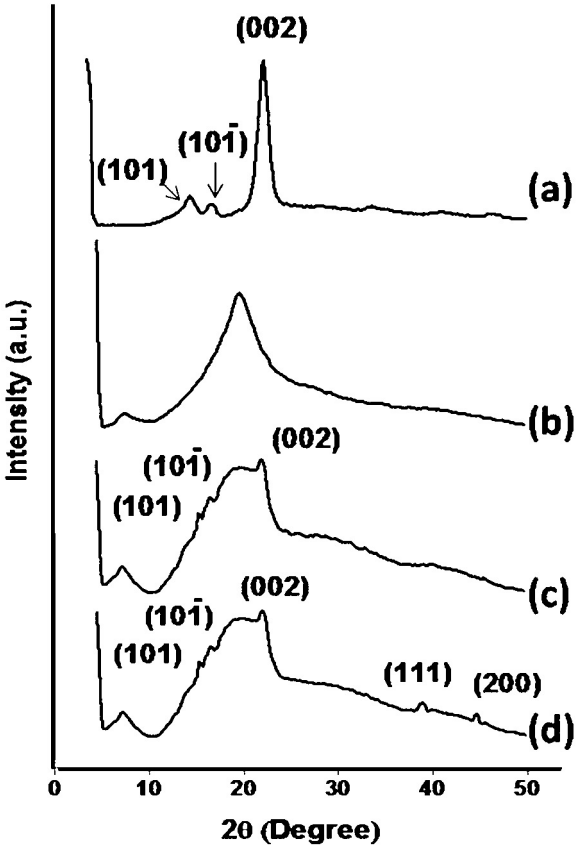

Fig. 5. XRD spectra of (a) BCNC, (b) HPMC, (c) HPMC + 4 wt% BCNC and (d) HPMC + 4 wt% BCNC + 1 wt% AgNPs.

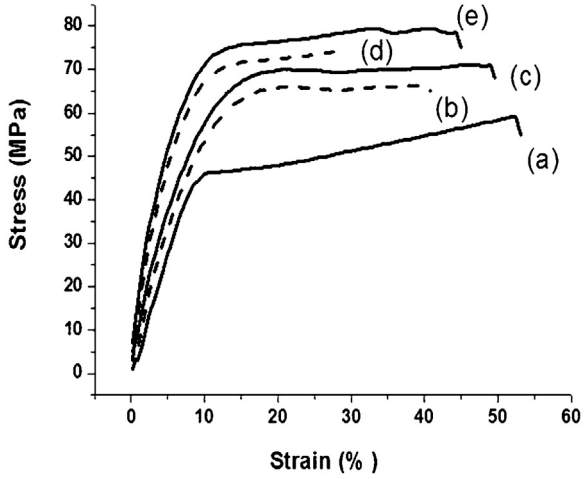

Fig. 6. Stress versus strain curves of (a) HPMC, (b) HPMC – 2% BCNC, (c) HPMC – 2% BCNC – 1% AgNPs, (d) HPMC – 4% BCNC and (e) HPMC – 4% BCNC – 1% AgNPs nanocomposites.

HPMC. X-ray diffraction pattern of HPMC nanocomposite containing 4 wt% of BCNC is shown in Fig. 5c. The changes observed in the diffraction pattern can be attributed to the presence of cellulose-I in BCNC, which also confirms the existence of BCNC in HPMC matrix. In the nanocomposites, the intensity of the diffraction peak of HPMC observed at 7.38° increased; while the peak at 19.65° became broader. This clearly indicated that the addition of BCNC had affected the crystalline nature of HPMC. The crystallinity index also increased from 64.5 to 66.3 by the addition of 4 wt% of BCNC (Table 1). Similarly the addition of AgNPs along with BCNC, resulted in the formation of two new peaks at 38.80° and 44.54° (Fig. 5d) corresponding to the (1 1 1) and (2 0 0) planes of the face-centered-cubic (fcc) silver, respectively (Sarkar et al., 2011). The addition of AgNPs has also increased the crystallinity index of HPMC.

3.5. Mechanical properties

The deformation patterns of HPMC and its nanocomposites containing both BCNC and AgNPs were shown in Fig. 6. The dotted line represents the HPMC nanocomposites containing 2 and 4 wt% of BCNC, while the solid line represents HPMC-BCNC nanocomposites containing 2 and 4 wt% of BCNC along with 1 wt% of AgNPs. AgNPs loaded nanocomposites exhibited improved strength and ductility compared to the nanocomposites without AgNPs. Tensile strength of HPMC improved from 59 MPa to 74 MPa upon adding 4 wt% of BCNC, while elongation at break reduced from 53.1% to 28.6% (Table 2). Cellulose nanocrystals are known to form a percolating network within the polymer matrix and the applied stress can be transferred through either filler–filler interaction or through filler–matrix interactions (Rusli, Shanmuganathan, Rowan, Weder, & Eichhorn, 2011). Since HPMC is also a hydrophilic polymer like bacterial cellulose, the possible interactions between matrix and filler will be predominant in these nanocomposites. These interactions will facilitate efficient load transfer between polymer chains and the percolating network of nanocrystals, which gives additional strength to the nanocomposites. In addition to tensile strength, other mechanical properties like modulus were also enhanced by the addition of BCNC, while elongation properties were decreased. The reduction in elongation properties is expected as BCNC, which is having interactions with HPMC can reduce the segmental mobility of HPMC chains. The increased brittleness exhibited by nanocomposites containing 4 wt% BCNC can also be attributed to the probable aggregation of the nanocrystals at higher concentrations which resulted in the formation of weak points. On the other hand, the addition of AgNPs affected the mechanical properties in a different way. AgNPs enhanced the tensile strength, modulus and percentage elongation of the nanocomposites. The addition of AgNPs resulted in increasing tensile strength to 71 MPa and 78 MPa for 2 and 4 wt% of BCNC, revealing the reinforcing capability of AgNPs. This may be because

Table 1
X-ray diffraction details of BCNC, HPMC and their nanocomposites.

Sample	Peak position(2θ)	d-spacing (A°)	Full width at half maximum	Average crystal size (A°)	Crystallinity index (%)
BCNC	15. 2	5.8	1.199	74.2	85.4
	17.4	5.2	0.887	100.6	
	22.7	3.9	1.322	68.1	
HPMC	7.4	11.7	1.552	57.0	64.5
	19.7	4.5	5.102	17.6	
HPMC + 4 wt%	7.4	11.7	1.610	54.9	66.3
BCNC	19.7	4.5	7.816	11.5	
HPMC + 4 wt%	7.4	11.7	1.613	54.8	68.4
BCNC + AgNPs	19.7	4.5	7.822	11.5	

Table 2
Mechanical properties of HPMC nanocomposites containing BCNC and AgNPs (*Mean ± SE, $n = 10$).

Sample	Thickness*(μm)	Tensile strength* (MPa)	Tensile modulus* (GPa)	Elongation at break* (%)
HPMC	202 ± 21	59 ± 5.3	1.33 ± 0.25	53.1 ± 5.7
HPMC + 2% BCNC	204 ± 19	66 ± 6.2	1.75 ± 0.23	43.8 ± 5.7
HPMC + 2% BCNC + 1% AgNPs	208 ± 10	71 ± 7.7	1.82 ± 0.25	49.7 ± 4.0
HPMC + 4% BCNC	210 ± 18	74 ± 8.1	2.13 ± 0.43	28.6 ± 4.8
HPMC + 4% BCNC + 1% AgNPs	246 ± 10	78 ± 6.9	2.28 ± 0.27	44.0 ± 4.5

AgNPs can have interactions with the OH groups of HPMC as observed in the FTIR studies, which can act as a physical crosslink and thereby increases the modulus and tensile strength. Similar improvement in tensile strength was reported in the case of HPMC based bactericidal nanocomposites containing silver nanoparticles previously (Moura, Mattoso, & Zucolotto, 2012). However, the main advantage of adding AgNPs lies in the enhanced ductility of these nanocomposites. The addition of 2 and 4 wt% of BCNC resulted in reducing elongation at break from 53.1% to 43.8% and 28.6% respectively; whereas, the addition of AgNPs helped to regain the lost properties to 49.7% and 44.0% respectively (Table 2). AgNPs and BCNC show opposite effects on elongation behaviour. AgNPs exhibit more interactions with the hydroxyl groups of both HPMC and BCNC and hence upon the formation of AgNPs, large numbers of OH groups of both HPMC and BCNC are presumably complexing with AgNPs and thereby reduced the interaction between HPMC and BCNC. Thus, the polymer chains are relatively free to move and can regain some of the lost elongation properties, without sacrificing on the other mechanical properties. Silver nanoparticles are very small size compared to cellulose nanocrystals and hence they can be accommodated within the interfacial regions of the polymer. The presence of such smaller particles within the polymer matrix does not contribute to the formation of additional weak points. Similar results were reported in the case of polyurethane containing bifunctional nanofillers (Liu, Song, Shang, Song, & Wang, 2012).

3.6. Moisture sorption analysis

Moisture sorption analysis of HPMC and its hybrid nanocomposites was carried out to study the effect of BCNC and AgNPs on the water vapour sorption at various relative humidity (RH) conditions. When a hydrophilic polymer like HPMC is exposed to different RH conditions it absorbs moisture until a state of equilibrium is reached, which is known as the equilibrium moisture content (EMC) at that particular RH. EMC of HPMC and its nanocomposites were determined at different RH conditions and plotted as sorption curves (Fig. 7A). The comparison of sorption curves revealed a difference in the moisture sorption rate of nanocomposites. The addition of BCNC reduced the moisture sorption of HPMC at RH conditions above 60%. This may be attributed to the presence of hydrogen bonds existing between the hydroxyl groups of BCNC and the hydroxyl groups of HPMC. These types of interactions can reduce the number of sorption sites available for moisture sorption in the polymer matrix, which ultimately reduces the EMC at higher RH. Similar effects were reported for galatomannan cellulose nanocomposites reinforced with cellulose nanowhiskers (Keating et al., 2013). Similarly the addition of AgNPs further reduced the moisture intake of these nanocomposites. AgNPs are having strong interactions with the hydroxyl groups of HPMC and BCNC, which minimises the interaction of water with the nanocomposites. The incorporation of two nanomaterials like BCNC and AgNPs together in a polymer matrix proved to be a simple technique to reduce the moisture affinity of hydrophilic polymers like HPMC, without compromising on any of the original properties of HPMC.

The experimental data obtained from the sorption studies were used to fit into five different kinetic models to study the dependence of equilibrium moisture content on the relative humidity in detail. The sorption models are useful for predicting moisture sorption properties of nanocomposite films, giving more information about the sorption pattern and the type of interactions existing between water molecules and cellulose materials. Three two-parameter models (Iglesias and Chirife, Smith and Caurie), one three-parameter model (Guggenheim-Anderson-de Boer) and one four-parameter model (Peleg) was selected to find out which mathematical model is fitting adequately for the nanocomposite films. The selected equations are detailed in Table 3. Sorption isotherm curves for HPMC and its nanocomposites fitting with Iglesias and Chirife, Smith, Caurie, GAB and Peleg models are represented in Fig. 7(B–F). The corresponding values of constants pertaining to each model were determined separately. The goodness of the fit of each model was computed with a coefficient of determination (R^2) from the experimental and predicted values as given in Table 4. Examination of the fitting data (R^2) revealed that Iglesias and Chirife, Smith and Caurie models failed to adequately describe the experimental data of HPMC and its nanocomposites, while GAB and Peleg models were able to give a reasonably good fit. Among all the five models, Peleg model was shown to give the closest fit to the experimental data giving an R^2 value in the range 0.997–0.998.

In the case of HPMC, the values of Peleg constants "*A*", and "*B*" found to be 21.83 and 1.42 respectively (Table 4). Peleg constant "*A*" relates to the sorption rate at the very beginning of the sorption process while the constant "*B*" relates to the maximum attainable moisture content (Peleg, 1993). Samples exhibiting lower "*B*" value will have a higher water absorption capacity. The addition of 2 and 4 wt% of BCNC resulted in decreasing the "*A*" value to 20.81 and 19.78, while "*B*" value increased to 1.52 and 1.71 respectively. This implies that the addition of BCNC increased the initial water absorption rate but at higher RH it reduced the moisture absorption capability. This result is in correlation with the explanation that the interaction between BCNC and HPMC is the main reason for reduced moisture absorption. The addition of AgNPs in the nanocomposites has not affected the "*A*" value significantly, but the "*B*" values were increased to 1.87 and 1.96 respectively. This suggests that AgNPs are not affecting the initial water absorption rate but at higher RH it reduced the moisture absorption capability considerably. The main advantage of this type of mathematical modelling is to save time in predicting the sorption kinetics and equilibrium moisture content using short time experimental data. This type of analysis

Table 3
Various sorption models used to fit the experimental values (X is the moisture content of the material on dry basis, X_0 is the monolayer moisture content, A, B, C, D are constants and a_w is water activity).

Model	Equation	Constants
Iglesias and Chirife	$X = A + B\{a_w/(1 - a_w)\}$	A, B
Smith	$X = A + B \times \log(1 - a_w)$	A, B
Caurie	$\ln X = A + Ba_w$	A, B
Guggenheim-Anderson-de Boer	$X = X_0KCa_w/[(1 - Ka_w)(1 - Ka_w + CKa_w)]$	X_0, K, C
Peleg	$X = Aa_w{}^B + Ca_w{}^D$	A, B, C, D

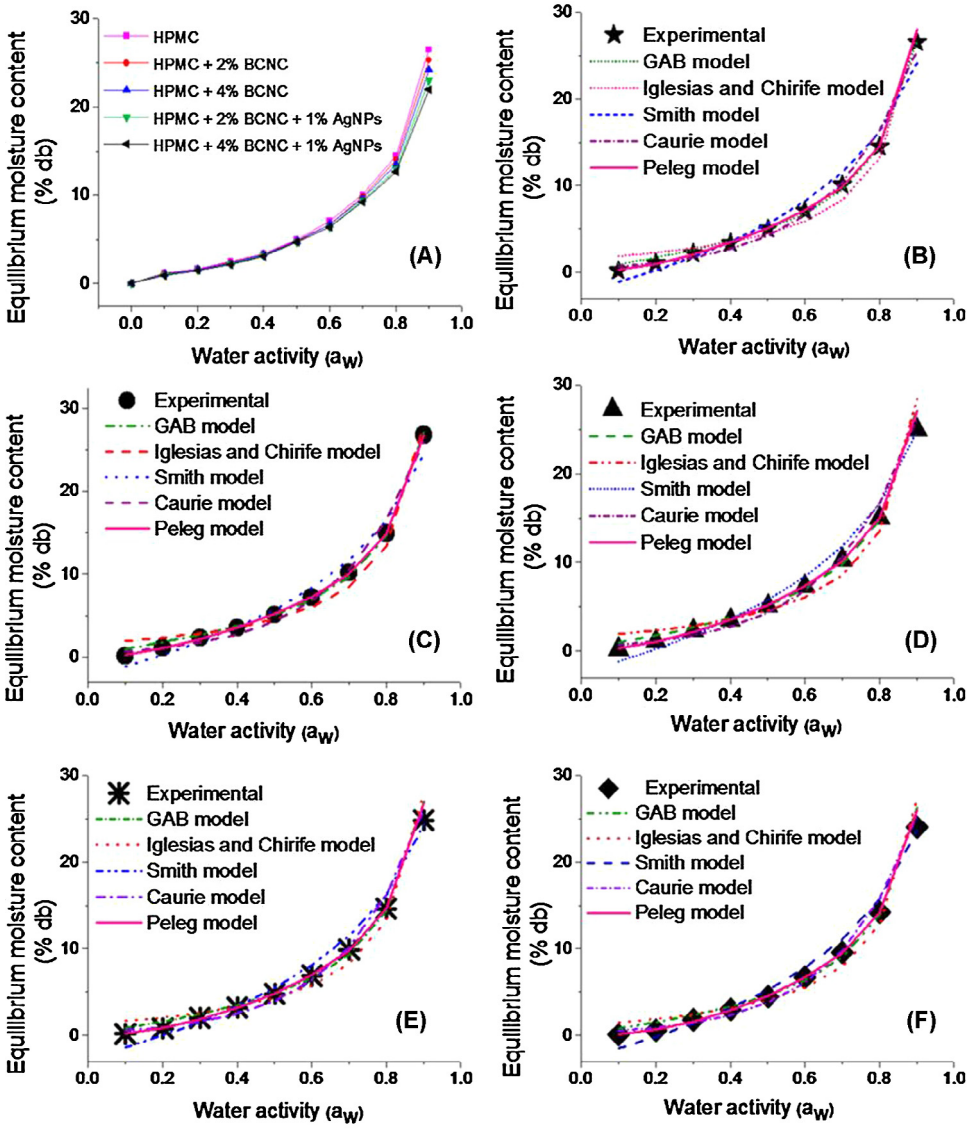

Fig. 7. (A) Overlay of moisture sorption isotherms of HPMC and its nanocomposites and individual sorption isotherms of (B) HPMC and HPMC nanocomposites containing (C) 2% BCNC, (D) 2% BCNC + 1 wt% AgNPs, (E) 4% BCNC and (F) 4% BCNC + 1 wt% AgNPs with various models obtained through experiment (with symbol) and predicted values (lines).

Table 4
Moisture sorption isotherm model constants and R^2 values for HPMC–BCNC nanocomposite films.

Empirical models		HPMC	HPMC + 2% BCNC	HPMC + 4% BCNC	HPMC + 2% BCNC + 1% AgNPs	HPMC + 4% BCNC + 1% AgNPs
Iglesias and Chirife	A	3.37 ± 0.91	3.10 ± 0.88	2.62 ± 0.89	2.18 ± 0.91	1.89 ± 0.86
model	B	2.77 ± 0.26	2.82 ± 0.25	2.84 ± 0.26	2.91 ± 0.26	2.94 ± 0.25
	R^2	0.939	0.946	0.942	0.941	0.947
Smith	A	−0.64 ± 0.35	−0.89 ± 0.43	−1.41 ± 0.38	−1.88 ± 0.39	−1.96 ± 0.45
model	B	11.32 ± 0.32	11.59 ± 0.38	11.68 ± 0.34	11.81 ± 0.35	11.95 ± 0.40
	R^2	0.954	0.952	0.953	0.953	0.951
Caurie	A	−0.01 ± 0.15	−0.07 ± 0.16	−0.14 ± 0.17	−0.23 ± 0.16	−0.35 ± 0.17
model	B	3.44 ± 0.18	3.55 ± 0.20	3.75 ± 0.21	3.83 ± 0.20	3.97 ± 0.21
	R^2	0.988	0.987	0.989	0.987	0.987
GAB model	X_0	0.18 ± 0.12	0.15 ± 0.14	0.11 ± 0.15	0.13 ± 0.15	0.09 ± 0.20
	B	0.92 ± 0.27	0.93 ± 0.26	0.96 ± 0.34	0.95 ± 0.29	0.97 ± 0.24
	C	0.061 ± 0.002	0.058 ± 0.002	0.055 ± 0.003	0.056 ± 0.002	0.051 ± 0.002
	R^2	0.9940	0.9945	0.9907	0.9931	0.9936
Peleg model	A	21.83 ± 0.58	20.81 ± 0.66	19.78 ± 0.55	20.79 ± 0.67	19.77 ± 0.71
	B	1.42 ± 0.04	1.52 ± 0.04	1.71 ± 0.04	1.87 ± 0.03	1.96 ± 0.04
	C	36.48 ± 3.36	43.87 ± 4.26	46.55 ± 7.57	51.44 ± 6.80	54.14 ± 6.36
	D	12.80 ± 1.17	14.80 ± 1.27	16.48 ± 1.89	17.61 ± 1.84	18.94 ± 1.69
	R^2	0.998	0.998	0.998	0.997	0.997

also helps to use water molecules as a probe to study the effect of nanomaterials on the polymer properties on a molecular scale.

4. Conclusion

HPMC based hybrid nanocomposite films were prepared by using a unique combination of two nanomaterials. AFM and TEM images together with UV–vis analysis was used to confirm the existence of both cellulose nanocrystals as well as silver nanoparticles within the polymer matrix. FTIR analysis was used to study the interaction of these nanomaterials with the polymer matrix, which concluded that the addition of BCNC enhanced the hydrogen bonding interactions with HPMC. It also revealed that AgNPs are strongly interacting with the hydroxyl groups of both HPMC and BCNC, making it unavailable for other molecules like water to interact. X-ray diffraction analysis clearly indicated that the addition of BCNC had affected the crystalline nature of HPMC, while AgNPs also contributed to improve the overall crystallinity of the nanocomposite films. The cellulose nanocrystals improved the mechanical properties like tensile strength and modulus of HPMC, while it reduced the elongation properties. On the other hand, the introduction of AgNPs helped to regain the lost elongation properties without compromising the other mechanical properties. The moisture sorption properties of these nanocomposites were also analyzed and the addition of AgNPs was found to significantly reduce the moisture absorption capability of these nanocomposites. Five, different mathematical models were used to fit the experimental data and among them Peleg model was found to be the best fitting model suitable for these types of nanocomposite films. A synergistic effect on the overall properties of HPMC nanocomposites was observed by combining two nanomaterials, which can be beneficial in making eco-friendly materials with improved properties for various applications.

Acknowledgements

The authors thank Dr H. V. Batra, Director DFRL, Mysore for constant support and encouragement. The authors are also thankful to JNCASR, Bangalore for their help in TEM analysis.

References

Ayranci, E., & Tunc, S. (2001). The effect of fatty acid content on water vapor and carbon dioxide transmission of cellulose-based edible films. *Food Chemistry*, *72*, 231–236.

Bertuzzi, M. A., Armada, M., & Gottifredi, J. C. (2007). Physicochemical characterization of starch based films. *Journal of Food Engineering*, *82*(1), 17–25.

Brindle, L. P., & Krochta, J. M. (2008). Physical properties of whey protein hydroxypropyl methylcellulose blend edible films. *Journal of Food Science*, *73*, 446–454.

Dogan, N., & McHugh, T. H. (2007). Effects of microcrystalline cellulose on functional properties of hydroxy propyl methyl cellulose microcomposite films. *Journal of Food Science*, *72*, E16–E22.

Fahs, A., Brogly, M., Bistac, S., & Schmitt, M. (2010). Hydroxypropyl methylcellulose (HPMC) formulated films: Relevance to adhesion and friction surface properties. *Carbohydrate Polymers*, *80*, 105–114.

George, J., Ramana, K. V., Sabapathy, S. N., Jagannath, J. H., & Bawa, A. S. (2005). Characterization of chemically treated bacterial (Acetobacter xylinum) biopolymer: Some thermo-mechanical properties. *International Journal of Biological Macromolecules*, *37*, 189–194.

George, J., Sajeevkumar, V. A., Kumar, R., Ramana, K. V., Sabapathy, S. N., & Bawa, A. S. (2008). Enhancement of thermal stability associated with the chemical treatment of bacterial (*Gluconacetobacter xylinus*) cellulose. *Journal of Applied Polymer Science*, *108*, 1845–1851.

George, J., Sajeevkumar, V. A., Ramana, K. V., Sabapathy, S. N., & Siddaramiah. (2012). Augmented properties of PVA hybrid nanocomposites containing cellulose nanocrystals and silver nanoparticles. *Journal of Materials Chemistry*, *22*, 22433–22439.

George, J., & Siddaramaiah. (2012). High performance edible nanocomposite films containing bacterial cellulose nanocrystals. *Carbohydrate Polymers*, *87*, 2031–2037.

Habibi, Y., Lucia, L. A., & Rojas, O. J. (2010). Cellulose nanocrystals: Chemistry, self-assembly, and applications. *Chemical Reviews*, *110*(6), 3479–3500.

Iguchi, M., Yamanaka, S., & Budhino, A. (2000). Review bacterial cellulose – A master piece of nature's art. *Journal of Material Science*, *35*, 261–270.

Keating, B. A., Hill, C. A. S., Sun, D., English, R., Davies, P., & McCue, C. (2013). The water vapor sorption behavior of a galactomannan cellulose nanocomposite film analyzed using parallel exponential kinetics and the Kelvin–Voigt viscoelastic model. *Journal of Applied Polymer Science*, *129*, 2352–2359.

Krochta, J. M., & Mulder-Johnston, C. (1997). Edible and biodegradable polymer films: Challenges and opportunities. *Food Technology*, *51*(2), 61–75.

Liu, H., Song, J., Shang, S., Song, Z., & Wang, D. (2012). Cellulose nanocrystal/silver nanoparticle composites as bifunctional nanofillers within waterborne polyurethane. *ACS Applied Materials & Interfaces*, *4*, 2413–2419.

Moura, De, M. R., Mattoso, L. H. C., Zucolotto, & V. (2012). Development of cellulose-based bactericidal nanocomposites containing silver nanoparticles and their use as active food packaging. *Journal of Food Engineering*, *109*, 520–524.

Pandey, J. K., Nakagaito, A. N., & Takagi, H. (2013). Fabrication and applications of cellulose nanoparticle-based polymer composites. *Polymer Engineering and Science*, *53*(1), 1–8.

Peleg, M. (1993). Assessment of a semi empirical four parameter general model for sigmoid moisture sorption isotherms. *Journal of Food Process Engineering*, *16*, 21–37.

Phan, T. D., Debeaufort, F., Peroval, C., Despre, D., Courthaudon, J. L., & Voilley, A. (2002). Arabinoxylan-lipids-based edible films and coatings. 3. Influence of drying temperature on film structure and functional properties. *Journal of Agriculture and Food Chemistry*, *50*, 2423–2428.

Rusli, R., Shanmuganathan, K., Rowan, S. J., Weder, C., & Eichhorn, S. J. (2011). Stress transfer in cellulose nanowhiskers composites-influence of whisker aspect ratio and surface charge. *Biomacromolecules*, *12*, 1363–1369.

Sarkar, P., Pyne, S., Sahoo, G. P., Bhui, D. K., Bar, H., Samanta, S., & Misra, A. (2011). Solution-phase synthesis of silver nanodiscs in HPMC-matrix and simulation of UV–vis extinction spectra using DDA based method. *Spectrochimica Acta Part A*, *82*, 368–374.

Sebti, I., Delves-Broughton, J., & Coma, V. (2003). Physicochemical properties and bioactivity of nisin-containing cross-linked hydroxypropylmethylcellulose films. *Journal of Agriculture and Food Chemistry*, *51*, 6468–6474.

Shanmuganathan, K., Capadona, J. R., Rowan, S. J., & Weder, C. (2010). Biomimetic mechanically adaptive nanocomposites. *Progress in Polymer Science*, *35*, 212–222.

Sorrentino, A., Gorrasi, G., & Vittoria, V. (2007). Potential perspectives of bio-nanocomposites for food packaging applications. *Trends in Food Science and Technology*, *18*(2), 84–95.

Tai, C. Y., Wang, Y.-H., Tai, C.-T., & Liu, H.-S. (2009). Preparation of silver nanoparticles using a spinning disc reactor in continuous mode. *Industrial Engineering Chemistry and Research*, *48*(22), 10104–10109.

Villalobos, R., Hernandez-Munoz, P., & Chiralt, A. (2006). Effect of surfactants on water sorption and barrier properties of hydroxypropyl methylcellulose films. *Food Hydrocolloids*, *20*, 502–509.

Wang, L., Dong, W., & Xu, Y. (2007). Synthesis and characterization of hydroxypropyl methylcellulose and ethyl acrylate graft copolymers. *Carbohydrate Polymers*, *68*, 626–636.

Xu, X., Liu, F., Jiang, L., Zhu, J. Y., Haagenson, D., & Wiesenborn, D. P. (2013). Cellulose nanocrystals vs. cellulose nanofibrils: A comparative study on their microstructures and effects as polymer reinforcing agents. *ACS Applied Materials and Interfaces*, *5*, 2999–3009.

Yao, R., Xu, J., Lu, X., & Deng, S. (2011). Phase transition behaviour of HPMC-AA and preparation of HPMC-PAA nanogels. *Journal of Nanomaterials*, 6 pages.